AMERICAN SOCIETY FOR MICROBIOLOGY | Journal of Virology®

PATHOGENESIS AND IMMUNITY

Enterovirus A71 Infection Activates Human Immune Responses and Induces Pathological Changes in Humanized Mice

Yanyan Ke,[a,b] Wai Nam Liu,[a] Zhisheng Her,[a] Min Liu,[a] Sue Yee Tan,[a] Yong Wah Tan,[a] Xue Ying Chan,[a] Yong Fan,[c] Edwin Kunxiang Huang,[d] Huiyi Chen,[e] Kenneth Tou En Chang,[e] Jerry Kok Yen Chan,[d,f] Justin Jang Hann Chu,[a,g] Qingfeng Chen[a,c,h]

[a]Institute of Molecular and Cell Biology, Agency for Science, Technology and Research, Singapore
[b]Department of Basic Medical Science, Xiamen Medical College, Fujian, China
[c]Key Laboratory for Major Obstetric Diseases of Guangdong Province, The Third Affiliated Hospital of Guangzhou Medical University, Guangzhou, China
[d]Department of Reproductive Medicine, KK Women's and Children's Hospital, Singapore
[e]Department of Pathology and Laboratory Medicine, KK Women's and Children's Hospital, Singapore
[f]Experimental Fetal Medicine Group, Yong Loo Lin School of Medicine, National University of Singapore, Singapore
[g]Department of Microbiology and Immunology, Yong Loo Lin School of Medicine, National University of Singapore, Singapore
[h]Department of Physiology, Yong Loo Lin School of Medicine, National University of Singapore, Singapore

ABSTRACT Since the discovery of enterovirus A71 (EV-A71) half a century ago, it has been recognized as the cause of large-scale outbreaks of hand-foot-and-mouth disease worldwide, particularly in the Asia-Pacific region, causing great concern for public health and economic burdens. Detailed mechanisms on the modulation of immune responses after EV-A71 infection have not been fully known, and the lack of appropriate models hinders the development of promising vaccines and drugs. In the present study, NOD-*scid IL2Rγ*$^{-/-}$ (NSG) mice with a human immune system (humanized mice) at the age of 4 weeks were found to be susceptible to a human isolate of EV-A71 infection. After infection, humanized mice displayed limb weakness, which is similar to the clinical features found in some of the EV-A71-infected patients. Histopathological examination indicated the presence of vacuolation, gliosis, or meningomyelitis in brain stem and spinal cord, which were accompanied by high viral loads detected in these organs. The numbers of activated human CD4$^+$ and CD8$^+$ T cells were upregulated after EV-A71 infection, and EV-A71-specific human T cell responses were found. Furthermore, the secretion of several proinflammatory cytokines, such as human gamma interferon (IFN-γ), interleukin-8 (IL-8), and IL-17A, was elevated in the EV-A71-infected humanized mice. Taken together, our results suggested that the humanized mouse model permits insights into the human immune responses and the pathogenesis of EV-A71 infection, which may provide a platform for the evaluation of anti-EV-A71 drug candidates in the future.

IMPORTANCE Despite causing self-limited hand-food-and-mouth disease in younger children, EV-A71 is consistently associated with severe forms of neurological complications and pulmonary edema. Nevertheless, only limited vaccines and drugs have been developed over the years, which is possibly due to a lack of models that can more accurately recapitulate human specificity, since human is the only natural host for wild-type EV-A71 infection. Our humanized mouse model not only mimics histological symptoms in patients but also allows us to investigate the function of the human immune system during infection. It was found that human T cell responses were activated, accompanied by an increase in the production of proinflammatory cytokines in EV-A71-infected humanized mice, which might contribute to the exacerbation of disease pathogenesis. Collectively, this model allows us to delineate the

Citation Ke Y, Liu WN, Her Z, Liu M, Tan SY, Tan YW, Chan XY, Fan Y, Huang EK, Chen H, En Chang KT, Chan JKY, Hann Chu JJ, Chen Q. 2019. Enterovirus A71 infection activates human immune responses and induces pathological changes in humanized mice. J Virol 93:e01066-18. https://doi.org/10.1128/JVI.01066-18.

Editor Susana López, Instituto de Biotecnologia/UNAM

Address correspondence to Qingfeng Chen, qchen@imcb.a-star.edu.sg.

Y.K. and W.N.L. contributed equally to this work.

J.J.H.C. and Q.C. are co-senior authors.

Received 19 June 2018
Accepted 5 November 2018
Accepted manuscript posted online 14 November 2018
Published 17 January 2019

modulation of human immune responses during EV-A71 infection and may provide a platform to evaluate anti-EV-A71 drug candidates in the future.

KEYWORDS enterovirus A71, human immune responses, humanized mice

Enterovirus A71 (EV-A71) is a nonenveloped, single-stranded, positive-sense RNA virus that belongs to human enterovirus A species of the *Enterovirus* genus, within the family *Picornaviridae* (1). Since its discovery in 1969 and initial description in 1974, EV-A71 has been regarded as one of the common causes of epidemics of hand-food-and-mouth disease (HFMD) (2, 3). Ever since then, outbreaks of EV-A71 infection have periodically occurred worldwide (2). More recently, epidemic and sporadic outbreaks of EV-A71 infection have been reported in the Asia-Pacific region, including China, Hong Kong, South Korea, and Taiwan (4–9).

In general, EV-A71 causes mild infection in children, which is usually asymptomatic, or may cause fever, diarrhea, rashes, herpangina, or HFMD (10). Although the initial viral infection is self-limited, it may be followed by acute flaccid paralysis, aseptic meningitis, meningoencephalitis, myocarditis, pulmonary edema, or a combination of these conditions (10–12). Notably, younger children less than 4 years old are more susceptible to severe forms of EV-A71-associated neurological diseases, such as meningitis, brain stem or cerebellar encephalitis, and poliomyelitis-like paralysis, and these neurological complications may occasionally result in permanent paralysis or even death (13–15). Recently, it was proposed that HFMD mainly affects infants and children rather than adults, which may be a consequence of weaker immune systems in infants and children (16). To date, a vast number of animal models, including nonhuman primates and small rodents, have been developed to determine the prevention, pathogenesis, and treatment of diseases caused by EV-A71. Nonetheless, each of these models has its corresponding limitations (17). EV-A71-infected rhesus monkeys developed neurological complications similar to those of humans, but this model is not suitable for the assessment of neurovirulence level. Moreover, this model is always associated with ethical and economic issues (18, 19). Neonatal mice were found to be susceptible to either mouse-adapted or non-mouse-adapted strains of EV-A71 (20–23). In addition, it was proposed that massive production of various proinflammatory cytokines, including mouse gamma interferon (IFN-γ), interleukin-1β (IL-1β), IL-6, IL-13, and tumor necrosis factor alpha (TNF-α), contribute to the pathogenicity of EV-A71 infection, which is in concordance with the clinical severity in EV-A71-infected patients (24–27). However, the immune system in neonatal mice has not yet matured, while adult mice are generally not susceptible to EV-A71 infection (17). Furthermore, the use of mouse-adapted EV-A71 strains may reduce the clinical relevance and hinders the development of vaccines and drugs (28). Therefore, appropriate animal models are warranted to dissect the precise immunopathological mechanisms for EV-A71 infection, which may facilitate the identification and screening of effective drug candidates.

In the present study, NOD-*scid IL2R*$\gamma^{-/-}$ (NSG) mice with human immune systems (here referred to as humanized mice) were successfully infected with a non-mouse-adapted strain of EV-A71. Four-week-old humanized mice after EV-A71 infection showed a decrease in neurobehavioral scores and displayed meningomyelitis and meningitis in brain and spinal cord, which were accompanied by an accumulation of virus in these organs. In addition, there was an increase in the number of activated human $CD4^+$ and $CD8^+$ T cells in the circulation and the spleen, and human EV-A71-specific T cell responses could be found in this model. Intriguingly, the secretion of various proinflammatory cytokines, including IFN-γ, IL-8, and IL-17A, was augmented, which may contribute to disease pathogenesis in the humanized mice after EV-A71 infection.

RESULTS

Four-week-old humanized mice are susceptible to EV-A71 infection. EV-A71 usually causes mild infections in children, and those who are younger than 4 years old are generally more susceptible to EV-A71 infection (15). The majority of animal studies also reported that younger mice, usually less than 3 weeks old, are more susceptible to EV-A71 infection (17). In the present study, humanized mice at different ages were infected intraperitoneally (i.p.) with 10^8 PFU of a non-mouse-adapted, human isolate EV-A71 strain 41, and their survival rate was recorded weekly. Ten-week-old humanized mice did not succumb to EV-A71 infection, with 100% survival and no observable clinical manifestations. Three- to 5-week-old humanized mice showed different susceptibilities to EV-A71 infection, with 3-week-old humanized mice showing the greatest susceptibility to EV-A71 infection, as reflected by the shortest life expectancy (Fig. 1A). Some clinical signs, including limb weakness and paralysis, were also observed in the EV-A71-infected mice. Nevertheless, 80% of the mice died within 2 weeks postinfection, and all of the mice died by the third week of infection. The survival rate of 4-week-old humanized mice decreased significantly after EV-A71 infection compared to that of the age-matched mock-infected humanized mice (Fig. 1A), which was 60% after 7 weeks of EV-A71 infection. On the other hand, 5-week-old humanized mice did not show significant change in their survival rate compared to that of their mock-infected counterparts. Hence, 4-week-old humanized mice were chosen as the model for the subsequent experiments. In addition, the survival rate of humanized mice was compared with that of the age-matched NSG mice after infection (Fig. 1B to E). It was found that the survival rate of the 3- and 4-week-old humanized mice was lower than that of their respective counterparts, suggesting a role of the human immune system in EV-A71 infection. In addition, limb paralysis was observed in the infected humanized mice within a week prior to death (data not shown). Using this criterion, mice were categorized as moribund (predicted to die) or surviving (predicted to survive). The neurobehavioral scores, which are determined by seven tests to evaluate the neurobehavioral function, decreased significantly in both groups of EV-A71-infected mice compared to those of the mock-infected mice (Fig. 1F; see also Table S1 in the supplemental material), indicating that humanized mice infected at 4 weeks of age showed a decrease in neurobehavioral function and displayed various clinical signs after EV-A71 infection.

Histopathological examination of the EV-A71-infected humanized mice. Severe forms of EV-A71-associated neurological complications were found in EV-A71-infected moribund mice, which are similar to those reported in patients, such as aseptic meningitis and brainstem and cerebellar encephalitis (29). The histopathological condition of EV-A71-infected surviving mice and moribund mice was examined by hematoxylin and eosin (H&E) staining. Extensive vacuolation, gliosis, or meningomyelitis was present in brain stem and spinal cord in the EV-A71-infected moribund mice (Fig. 2), which is similar to the pattern of EV-A71-induced acute flaccid paralysis in patients (30), and meningitis was also observed at the membrane of the cerebral cortex in the moribund mice. In addition, the presence of interstitial mononuclear cell infiltrate and polymorphonuclear cell infiltrate was observed in muscle and lung, respectively, and intra-alveolar hemorrhage was found in the moribund mice (Fig. 2). No observable pathological changes were present in other organs in the humanized mice after EV-A71 infection, and microscopic lesions were also absent from these organs.

Presence of EV-A71 in blood and in various organs in EV-A71-infected humanized mice. Blood samples were collected from mock-infected and EV-A71-infected humanized mice at regular intervals after infection, and quantitative PCR (qPCR) was performed for the detection of EV-A71 viremia. The EV-A71 titer in the blood of the moribund mice was higher, although there were no significant differences between the surviving mice and the moribund mice (Fig. 3A). Various organs from the mice were also harvested at different time points for the determination of viral loads. In moribund mice, the viral titers in some of the organs, such as the spinal cord and brain stem, were

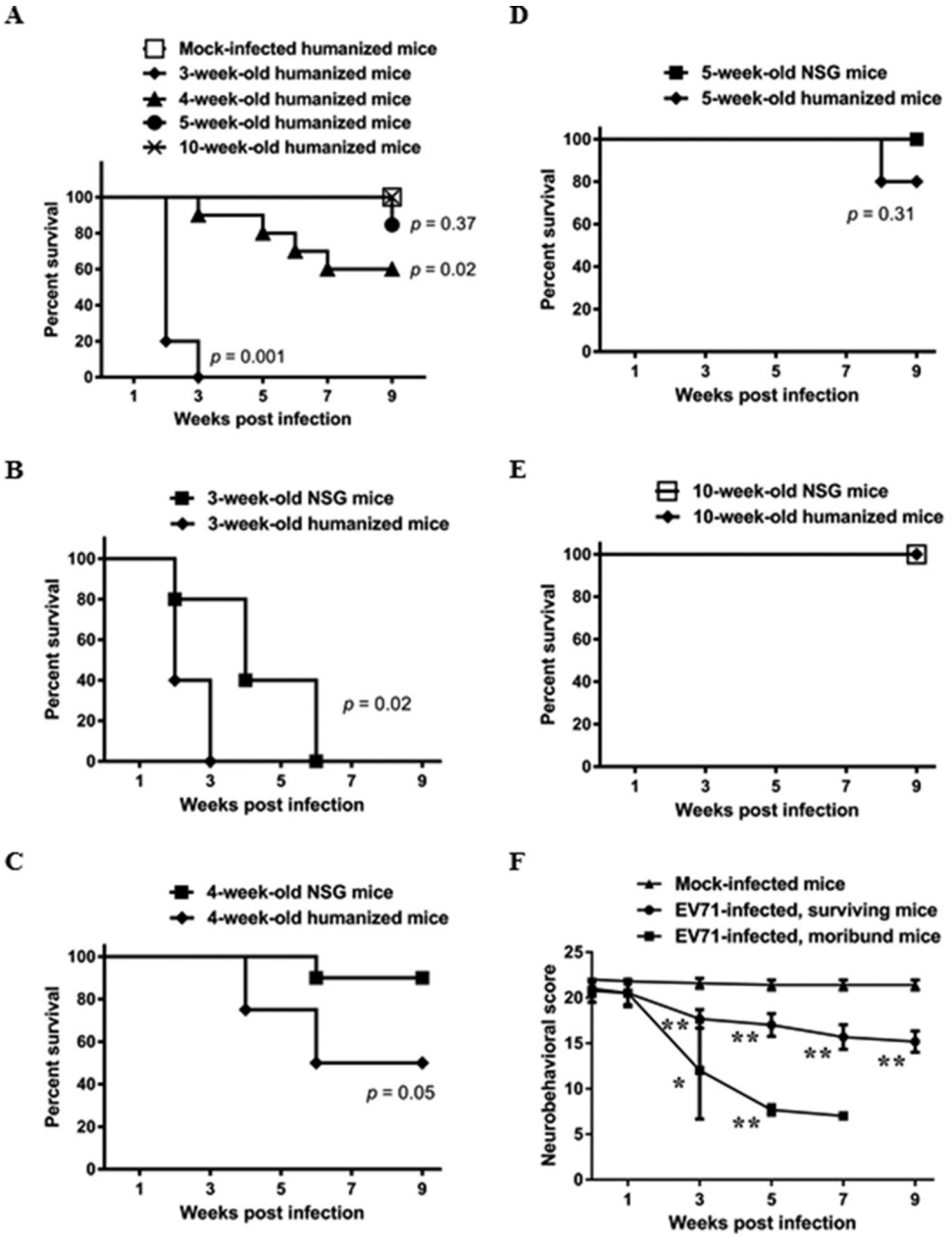

FIG 1 EV-A71 infection increases the mortality of humanized mice, accompanied by a decrease in the neurobehavioral scores. (A) Humanized mice at different ages were inoculated i.p. with or without EV-A71 (10^8 PFU/mouse). The survival rate of mock-infected mice ($n = 10$) and EV-A71-infected mice ($n = 10$ for 4-week-old and 5-week-old groups; $n = 5$ for the remaining groups) at the indicated weeks postinfection is shown. (B to E) Humanized mice and NSG mice at different ages were inoculated i.p. with EV-A71 (10^8 PFU/mouse). The survival rate of humanized mice ($n = 8$ for 4-week-old group; $n = 5$ for the remaining groups) and NSG mice ($n = 10$ for 4-week-old group; $n = 5$ for the remaining groups) at the indicated weeks postinfection is shown. The survival rate of mice between two groups is compared by Kaplan-Meier analysis via a log-rank test. (F) Humanized mice at 4 weeks of age were inoculated i.p. with or without EV-A71 (10^8 PFU/mouse). The neurobehavioral scores of mock-infected mice ($n = 10$), EV-A71-infected surviving mice ($n = 6$), and moribund mice ($n = 4$) at the indicated weeks postinfection are shown. Data are expressed as means ± SEM. *, $P < 0.05$; **, $P < 0.01$ (relative to the mock-infected group).

significantly higher than those in the surviving mice (Fig. 3B to D). Immunohistochemical (IHC) staining using an anti-EV-A71 monoclonal antibody, which stains the viral capsid protein VP1, confirmed that more viral particles were present in the organs of moribund mice than those in the surviving mice, while none of the organs from the mock-infected mice were positively stained with EV-A71 (Fig. 4).

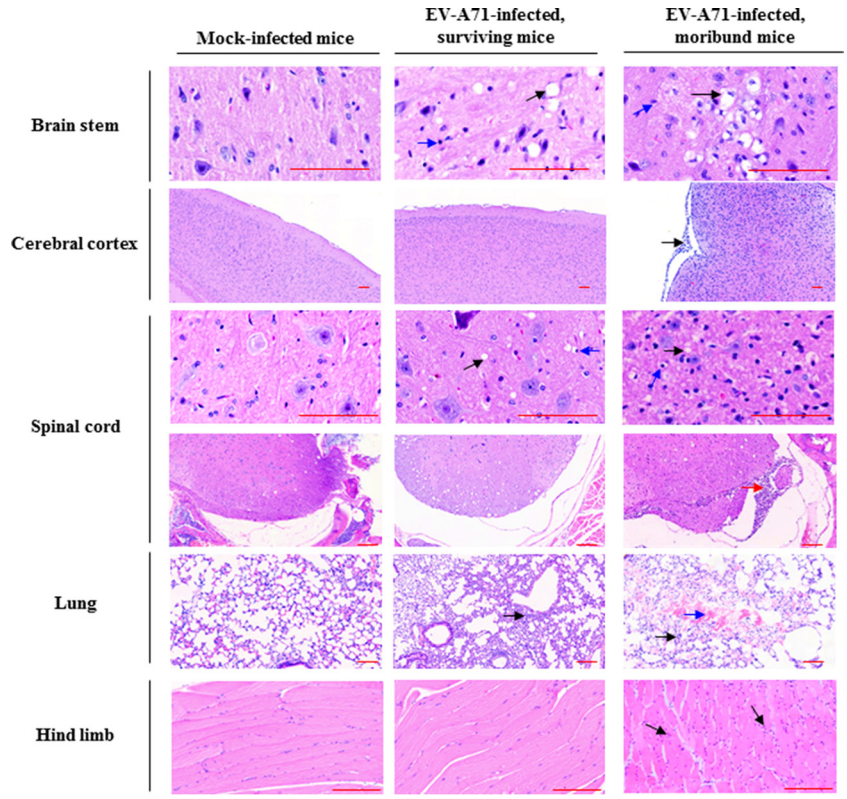

FIG 2 EV-A71 infection induces pathogenesis in various organs in humanized mice. Four-week-old humanized mice were inoculated i.p. with or without EV-A71 (10^8 PFU/mouse). Representative photomicrographs of H&E staining of different organs among mock-infected mice ($n = 5$), EV-A71-infected surviving mice ($n = 6$), and moribund mice ($n = 4$) are shown. Pathological changes were detected mainly in the organs of the EV-A71-infected moribund mice. Note the presence of vacuolation (black arrow) and gliosis (blue arrow) in brain stem; polymorphonuclear meningitis (black arrow) at the membrane of cerebral cortex; vacuolation (black arrow), gliosis (blue arrow), and polymorphonuclear or mononuclear meningomyelitis in spinal cord (red arrow); diffuse interstitial polymorphonuclear cell infiltrate (black arrow) and focal intra-alveolar hemorrhage (blue arrow) in lung; and focal interstitial mononuclear cell infiltrate (black arrow) in muscle. Bars, 100 μm.

EV-A71 infection activates human T cells. To investigate the numerical and phenotypical changes in human immune cells after EV-A71 infection, flow cytometric analysis on peripheral blood mononuclear cells from humanized mice was performed. As shown in Fig. 5A and B, the number of human immune cells, in particular human $CD3^+$ T cells, was elevated in the circulation after EV-A71 infection. It was found that $CD4^+$ and $CD8^+$ T cells were significantly increased between 3 and 7 weeks postinfection compared to levels for the mock-infected humanized mice (Fig. 5C and D). Intriguingly, 1 week after EV-A71 infection, there was a significant increase in the number of $CD4^+$ $CD69^+$ cells (Fig. 5E), which represents an early activation of the $CD4^+$ T cells, followed by an increase in the number of $CD4^+$ HLA-DR^+-activated T cells (Fig. 5F). Similarly, the number of $CD8^+$ $CD69^+$- and $CD8^+$ HLA-DR^+-activated T cells was upregulated at 3 weeks postinfection (Fig. 5G and H).

The immune cell profile of the spleen was also analyzed by flow cytometry. Notably, there was a significant increase in the number of $CD4^+$ $CD69^+$, $CD8^+$ $CD69^+$, and $CD8^+$ HLA-DR^+ T cells in the spleen after EV-A71 infection (Fig. 6A). Furthermore, human IFN-γ T cell enzyme-linked immunosorbent spot (ELISPOT) assay was carried out to determine the presence of EV-A71-specific human T cell responses. Splenocytes from mock-infected mice and EV-A71-infected mice were harvested and stimulated with UV-inactivated EV-A71, while splenocytes stimulated with phytohemagglutinin (PHA) served as a positive control. The number of IFN-γ-producing spot-forming units (SFU) was augmented in the splenocytes from the EV-A71-infected group, while the spleno-

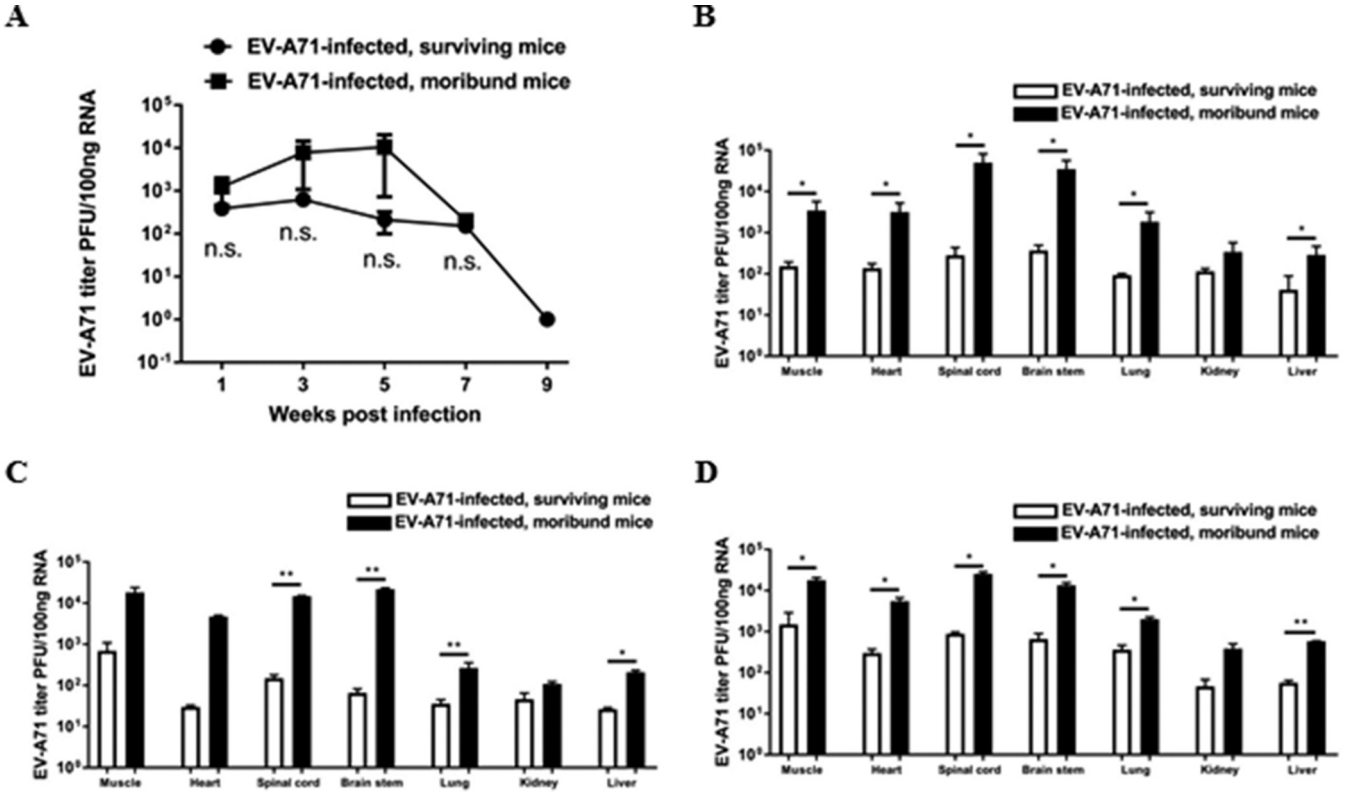

FIG 3 Detection of EV-A71 in blood and in various organs in humanized mice after infection. Four-week-old humanized mice were inoculated i.p. with or without EV-A71 (10^8 PFU/mouse). (A) Viral titers in the blood of surviving mice ($n = 4$) and moribund mice ($n = 4$) were determined by qPCR. Data are expressed as means ± SEM. n.s., not significant. (B) Viral titers in various organs of surviving mice ($n = 4$) and moribund mice ($n = 4$) at different endpoints were determined by qPCR. (C and D) Viral titers in different organs of surviving mice ($n = 2$ for each time point) and moribund mice ($n = 2$ for each time point) at 4 weeks (C) and 6 weeks (D) after EV-A71 infection are shown. Data are expressed as means ± SEM. *, $P < 0.05$; **, $P < 0.01$.

cytes from the mock-infected group barely responded to the inactivated EV-A71 (Fig. 6B and C), suggesting that the EV-A71-specific human T cell responses were present in this model.

EV-A71 infection leads to infiltration of human immune cells in various organs. An earlier report from Lin et al. demonstrated the infiltration of $CD20^+$ B cells as well as $CD4^+$ and $CD8^+$ T cells into the spinal cord from a patient with EV-A71 infection. In addition, infiltration of B cells and T cells was only observed in the brain of EV-A71-infected mice but not in the brain of mock-infected mice (31). To examine whether human immune cells were present in various organs after EV-A71 infection, flow cytometric analysis was performed. Consistent with the earlier report, there was a significant increase in the number of $CD45^+$, $CD3^+$, and $CD3^+$ $CD8^+$ T cells in the brain and the lung after EV-A71 infection, while the number of $CD3^+$ $CD4^+$ T cells and $CD14^+$ monocytes was also elevated in the brain (Fig. 7A and B). IHC staining, using an anti-human CD45 antibody, further revealed the infiltration of human $CD45^+$ cells in the brain and the spinal cord of the EV-A71-infected moribund mice. In contrast, no infiltration or minimal infiltration, if any, was found in the mock-infected mice and the EV-A71-infected surviving mice (Fig. 7C). On the other hand, more infiltrating human $CD45^+$ cells were present in the lung of the moribund mice than in the mock-infected mice and the surviving mice (Fig. 7C). Collectively, these results confirmed that human immune cells had infiltrated into the brain and lung in the EV-A71-infected humanized mice.

Upregulation of proinflammatory cytokine secretion in humanized mice after EV-A71 infection. It has been reported that the production of various cytokines is enhanced in patients after EV-A71 infection (32). To dissect human cytokine responses to EV-A71 infection, human IFN-γ, IL-8, and IL-17A levels in serum were monitored at

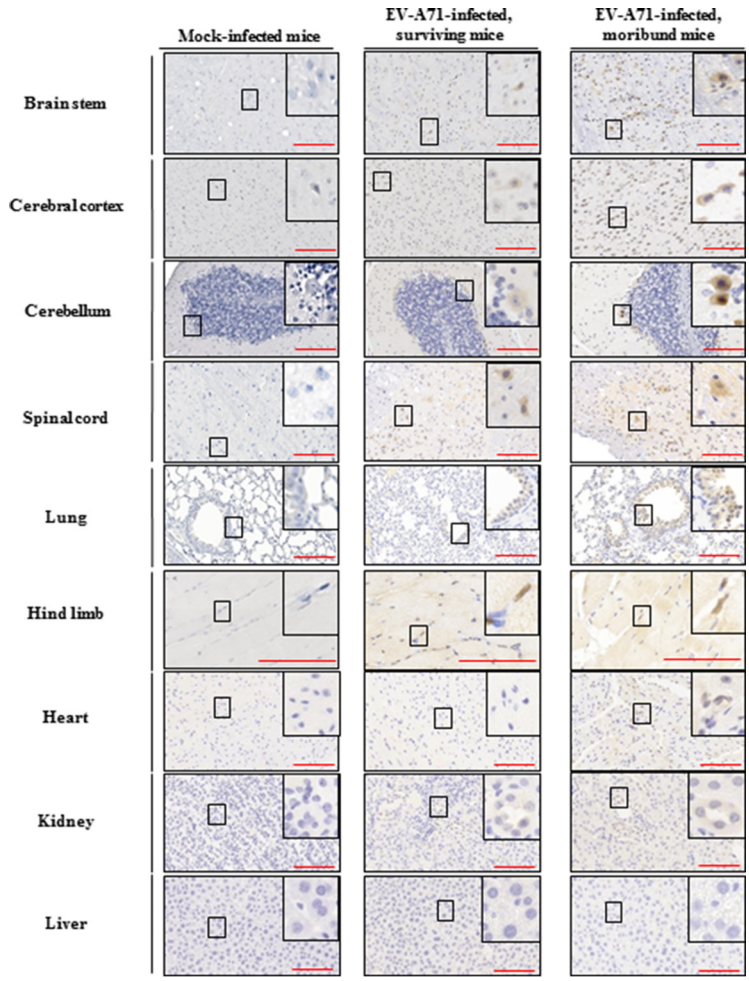

FIG 4 Presence of viral VP1 protein in various organs in humanized mice after EV-A71 infection. Four-week-old humanized mice were inoculated i.p. with or without EV-A71 (10^8 PFU/mouse). Representative photomicrographs of immunohistochemistry for different organs among mock-infected mice ($n = 5$), EV-A71-infected surviving mice ($n = 6$), and moribund mice ($n = 4$) are shown. VP1-positive signals were detected in different organs in the EV-A71-infected surviving mice and moribund mice. The boxes depict magnified areas. Bars, 100 μm.

regular intervals after infection. In concordance with the clinical studies, the level of the human proinflammatory cytokines, namely, IFN-γ and IL-8, was significantly upregulated in the EV-A71-infected humanized mice at 1 week postinfection (Fig. 8A and B). The serum level of IFN-γ and IL-8 in the infected mice was higher than that in the mock-infected mice until the experimental endpoint, although the increase in IL-8 level was not statistically significant at a later time point. Interestingly, the level of human IL-17A was also elevated after EV-A71 infection (Fig. 8C), which is in line with the finding of Chen et al., showing that the plasma IL-17 concentration was higher in EV-A71-infected patients than in healthy controls (33).

DISCUSSION

Since the discovery of EV-A71 in 1969, it has been recognized as the cause of large-scale outbreaks of HFMD worldwide, in particular in the Asia-Pacific region, causing great concern for public health and economic burdens (34). Currently, only limited EV-A71 vaccines are available worldwide, and anti-EV-A71 drugs are still under development for clinical treatment after infection (35–37). The major clinical signs of EV-A71 infection are HFMD and herpangina in children, although other members of *Enterovirus* can also cause HFMD in patients. Nevertheless, EV-A71 is associated with

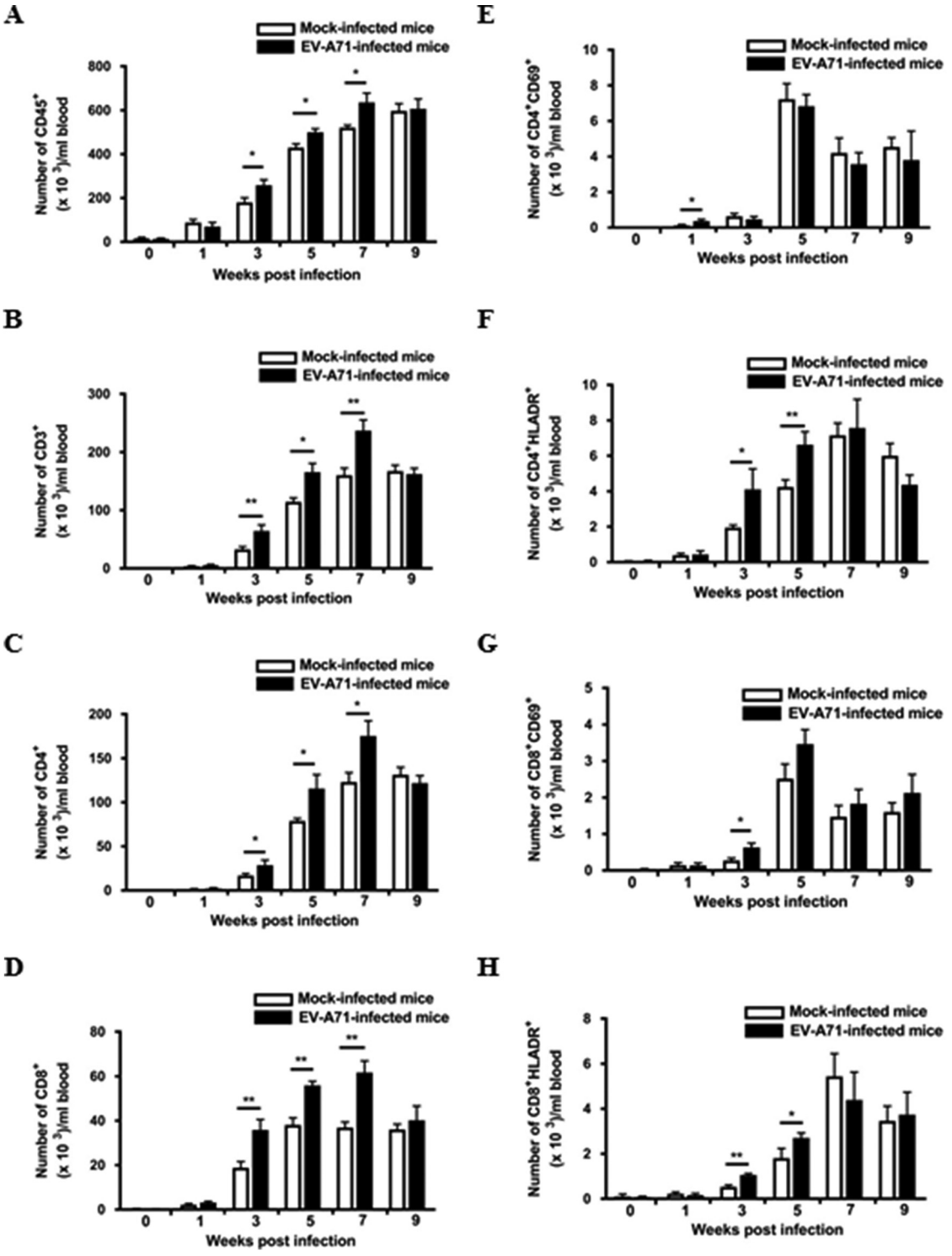

FIG 5 Activation of human T cell responses in the circulation of the EV-A71-infected humanized mice. Four-week-old humanized mice were inoculated i.p. with or without EV-A71 (10^8 PFU/mouse). (A to H) Blood samples from mock-infected ($n = 4$) and EV-A71-infected humanized mice ($n = 4$) were collected at the indicated weeks postinfection, and the cells were analyzed by flow cytometry. The total number of different immune cell types in the mice is indicated in the graphs. Data are expressed as means ± SEM. *, $P < 0.05$; **, $P < 0.01$.

severe forms of neurological diseases, including brainstem encephalitis, autonomic nervous system dysregulation, and pulmonary edema (12), and younger children are more susceptible to the severe forms of EV-A71-associated neurological diseases. Similarly, we demonstrated that younger humanized mice at the age of 4 weeks were

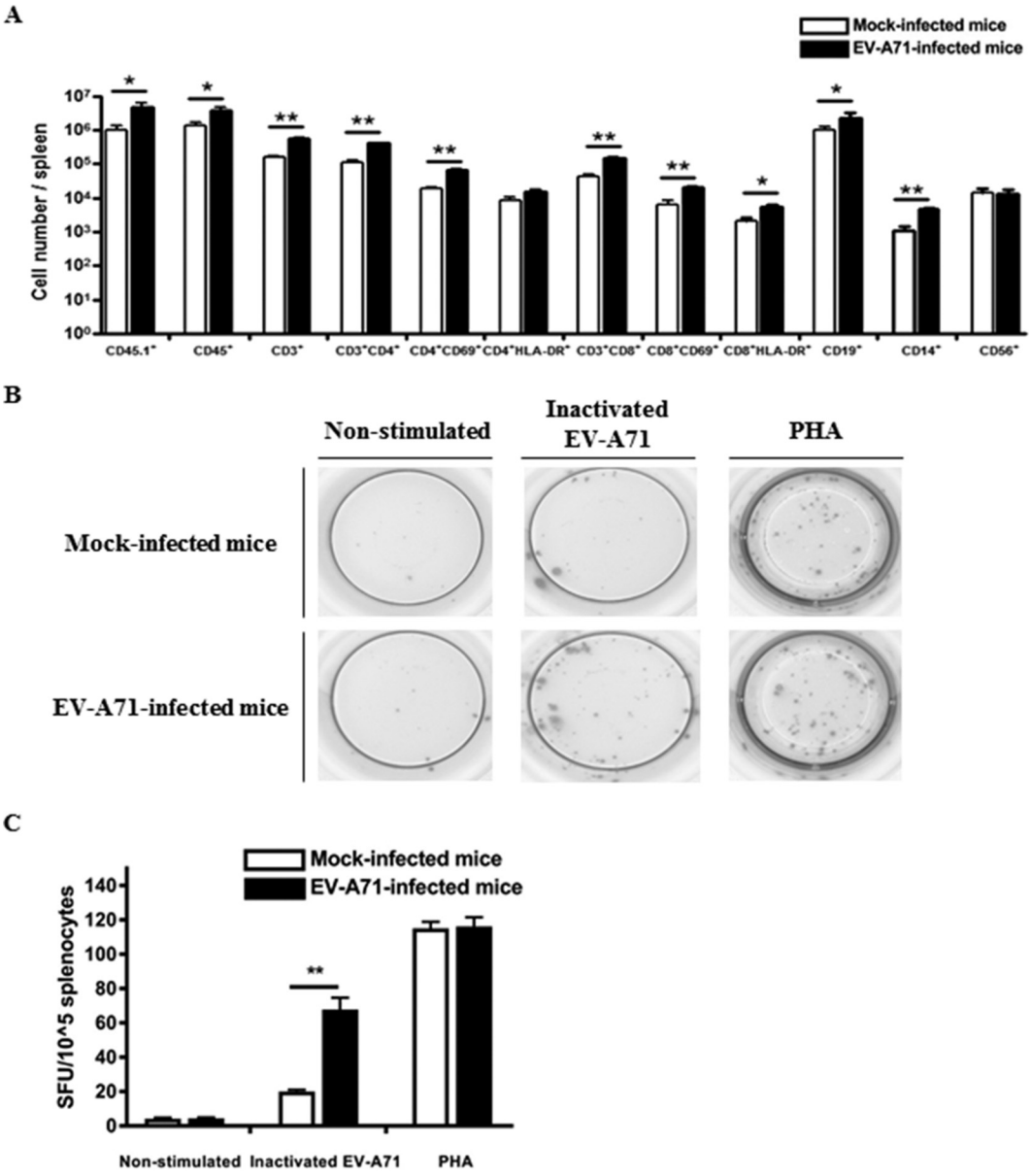

FIG 6 Activation of human T cells and the presence of EV-A71-specific T cell responses in the spleen of humanized mice after EV-A71 infection. Four-week-old humanized mice were inoculated i.p. with or without EV-A71 (10^8 PFU/mouse). (A) Mononuclear cells (MNC) were isolated from spleen at 9 weeks postinfection for FACS analysis. The total number of different immune cell types in the spleen of the mock-infected ($n = 4$) and EV-A71-infected humanized mice ($n = 4$) is indicated in the graph. Data are expressed as means ± SEM. *, $P < 0.05$; **, $P < 0.01$. (B and C) MNC from mock-infected ($n = 4$) and EV-A71-infected humanized mice ($n = 4$) were isolated from the spleen at 9 weeks postinfection, and 10^4 MNC were stimulated with inactivated EV-A71 for 72 h for human IFN-γ ELISPOT assay. Representative ELISPOT results for nonstimulated and inactivated EV-A71-stimulated MNC from mock-infected and EV-A71-infected humanized mice are shown. PHA-stimulated cells were used as a positive control. The human IFN-γ T cell responses from each group are shown as spot-forming units (SFU) per 10^4 MNC. Data are expressed as means ± SEM. **, $P < 0.01$.

more susceptible to the non-mouse-adapted strain of EV-A71 infection, whereas the mice at 10 weeks old did not succumb to the infection. Consistent with our findings, previous reports have shown that mice more than 4 weeks old generally were not susceptible to EV-A71 infection (17), while some studies reported that 10-week-old AG129 immunocompromised mice were susceptible to a mouse-adapted strain of EV-A71 infection, which might be the consequence of the mutation of VP1 protein (38, 39). In addition, we found that 4-week-old humanized mice were more susceptible to EV-A71 infection than age-matched EV-A71-infected NSG mice, as reflected by a

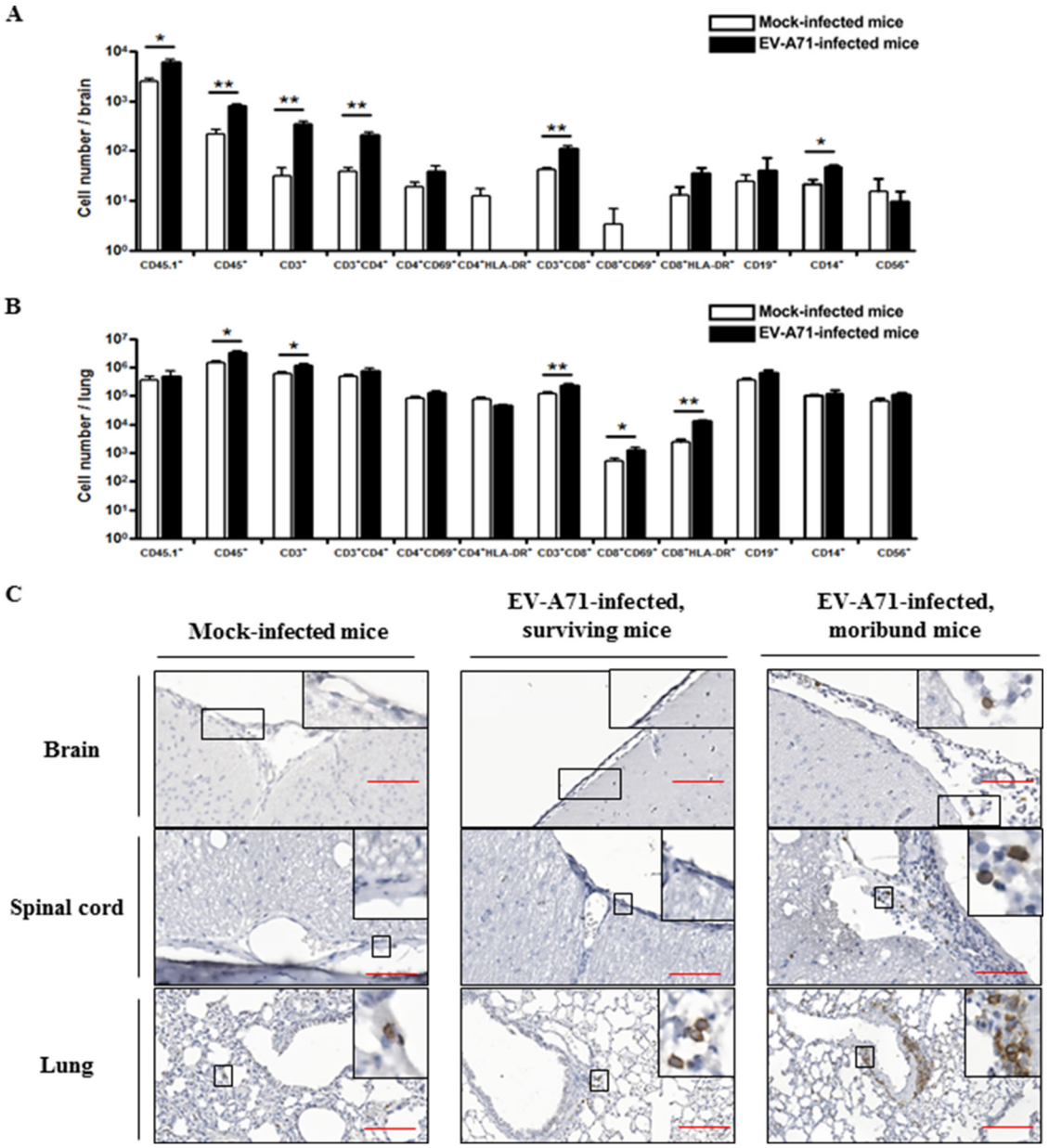

FIG 7 Infiltration of human CD45$^+$ immune cells in various organs in EV-A71-infected humanized mice. Four-week-old humanized mice were inoculated i.p. with or without EV-A71 (10^8 PFU/mouse). The total number of different immune cell types in the brain (A) and the lung (B) of the mock-infected ($n = 4$) and EV-A71-infected humanized mice ($n = 4$) is indicated in the graphs. Data are expressed as means ± SEM. *, $P < 0.05$; **, $P < 0.01$. (C) Representative photomicrographs of immunohistochemistry for different organs among mock-infected mice ($n = 5$), EV-A71-infected surviving mice ($n = 6$), and moribund mice ($n = 4$) are shown. Only a few human CD45$^+$ immune cells (black arrow) were present in the lung of the mock-infected mice, while the EV-A71-infected mice showed a marked increase in the number of infiltrating human CD45$^+$ cells in brain, spinal cord, and lung. The boxes depict magnified areas. Bars, 100 μm.

decrease in the survival rate of the humanized mice, suggesting a role of the human immune system in EV-A71 infection.

Similar to the clinical features in some of the EV-A71-infected patients, moribund mice after EV-A71 infection showed hind limb weakness and paralysis prior to death, accompanied by a significant decrease in neurobehavioral scores compared to those of the mock-infected mice. Histopathological examination further revealed the presence of vacuolation, gliosis, or meningomyelitis in brain stem and spinal cord, and meningitis was observed at the membrane of cerebral cortex in the EV-A71-infected moribund mice, suggesting that central nervous system (CNS) was infected by EV-A71, as ob-

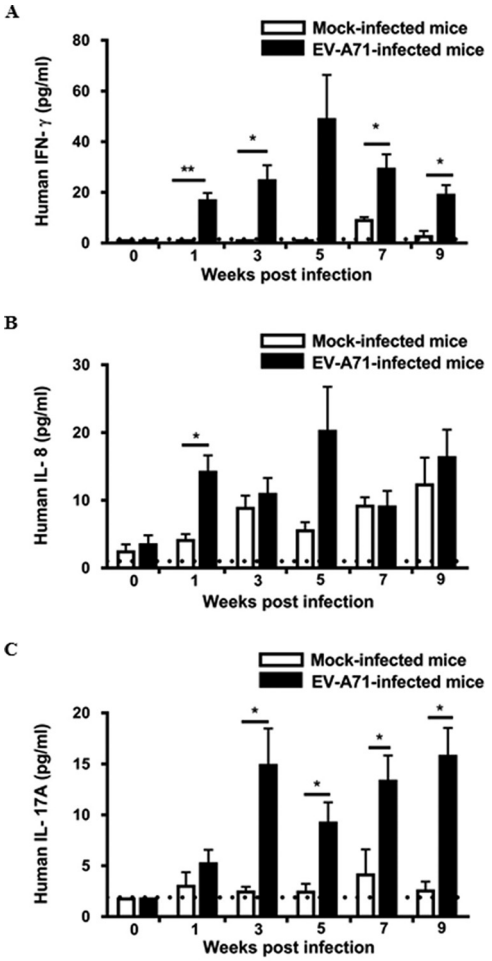

FIG 8 EV-A71 infection stimulates the secretion of proinflammatory cytokines in humanized mice. Four-week-old humanized mice were inoculated i.p. with or without EV-A71 (10^8 PFU/mouse). Serum samples were collected at the indicated weeks postinfection. Serum level of human IFN-γ (A), IL-8 (B), and IL-17A (C) was determined by a LEGENDplex human inflammation panel ($n = 4$ for mock-infected group; $n = 8$ for EV-A71-infected group). The dotted line in each graph represents the minimum detectable concentration of each cytokine. Data are expressed as means ± SEM. *, $P < 0.05$; **, $P < 0.01$.

served in humans. Intriguingly, pulmonary edema, which is a hallmark feature in EV-A71 patients with severe complications (40), was not observed in the EV-A71-infected humanized mice, despite the presence of interstitial mononuclear cell infiltrate and polymorphonuclear cell infiltrate and intra-alveolar hemorrhage in the mice. From our results, EV-A71-infected moribund mice showed a higher level of viremia than the surviving mice, although the difference was not statistically significant. This is in parallel with a clinical report which suggested that viremia does not have a significant impact on the distribution of clinical severity of EV-A71 cases (41). On the other hand, the virus exhibited strong neurotropism at the CNS in the EV-A71-infected moribund mice, in which the virus preferentially accumulated in the brain and the spinal cord. The high titer of virus found in the CNS might be one of the factors leading to the moribund status of the mice, and the neurotropism is consistent with the encephalomyelitis observed in EV-A71 patients (11). Apart from the brain and the spinal cord, EV-A71 was also detected in the lung and the hind limb, as indicated by IHC staining. Consistent with this finding, EV-A71-infected AG129 mice showed an accumulation of virus in the limb muscles (28). It is generally proposed that skeletal muscle supports enterovirus infection and the virus spreads from the muscle to the CNS through nervous pathways (28, 42), and our model is capable of demonstrating the systemic spread of EV-A71 into multiple organs, including the muscle, the spinal cord, and the brain of infected mice.

It has been suggested that cellular immunity, rather than humoral immunity, is associated with the clinical outcomes of EV-A71 infection (43). In addition, previous reports have shown that the number of circulating immune cells, including T follicular helper cells, type 1 helper and cytotoxic T cells, and T helper 17 and 22 cells, increases with the severity of HFMD after EV-A71 infection, accompanied by an increase in the secretion of various cytokines, such as IL-6, IL-17, IL-21, IL-22, and TNF-α (44–46). In another report, a decrease in the number of $CD4^+$ and $CD8^+$ T cells and NK cells was observed when the patients advanced from autonomic nervous system dysregulation to pulmonary edema (27), suggesting that cellular immunity is one of the factors that governs disease severity. In the present study, the number of human $CD45^+$, $CD3^+$, $CD4^+$, and $CD8^+$ cells was significantly increased in the humanized mice at 3 weeks to 7 weeks postinfection. Intriguingly, the number of activated T cells ($CD69^+$ or HLA-DR^+ T cells) was significantly upregulated within 5 weeks of EV-A71 infection, suggesting a role of activated T cells in the early phase of disease pathogenesis, which plausibly involved the secretion of inflammatory cytokines. Remarkably, HLA-DR is a human-specific molecule that is upregulated in human T cells and NK cells after activation (47, 48). Therefore, HLA-DR^+ T cells were present in our humanized mouse model after EV-A71 infection but was unlikely in other mouse models. Consistent with the profile of immune cells in the circulation, the number of activated T cells in the spleen was also elevated. In addition, the presence of EV-A71-specific human T cell responses also provided concrete evidence of EV-A71 infection in our humanized mice. Of note, the human immune system in the humanized mice is still naive when the mice were infected with EV-A71 at 4 weeks of age. On the one hand, the naive immune system in the mice is similar to the immature immune system in younger children, which allows us to investigate the modulation of the immune system after EV-A71 infection. On the other hand, careful interpretation of the immune response is required, as there is a lack of some immune cell subsets at the time of EV-A71 infection.

Additionally, infiltrating immune cells, including $CD4^+$ and $CD8^+$ T cells and $CD20^+$ B cells, were found in spinal cord in one fatally EV-A71-infected patient, which was accompanied by an increase in the viral load in brain (31). In the same study, EV-A71-infected neonatal mice, including ICR mice and C57BL/6 mice, possessed a higher number of infiltrating $CD4^+$ and $CD8^+$ T cells and $CD19^+$ B cells in their brain after the third day of infection than their uninfected counterparts (31). By flow cytometric analysis, our results revealed an elevation in the number of $CD4^+$ and $CD8^+$ human T cells in brain and lung after EV-A71 infection. Furthermore, there was a significant increase in the number of $CD14^+$ cells in the brain. It has been demonstrated that EV-A71 has the ability to replicate in $CD14^+$ cells, and the infected $CD14^+$ cells are capable of stimulating the proliferation of T cells and further stimulating the release of functional cytokines in rhesus monkeys (49). The functional role of $CD14^+$ cells in our humanized mouse model warrants further investigation.

The occurrence of brainstem encephalitis in EV-A71-infected patients was found to be associated with the local production of proinflammatory cytokines, and a number of clinical reports also suggested that an increase in serum IFN-γ, IL-6, IL-10, and IL-13 levels was associated with the development of pulmonary edema in the infected patients (27, 50, 51). In the current study, the secretion of various proinflammatory cytokines, including human IFN-γ, IL-8, and IL-17A, was stimulated in the EV-A71-infected humanized mice, while there were no significant changes in the IL-6 level in blood. In particular, IFN-γ and IL-6 are thought to be involved in the development of pulmonary edema in mice during EV-A71 infection (24, 25), although the role of IFN-γ is still undetermined (52, 53). In the EV-A71-infected humanized mice, there was only a subtle increase in the IFN-γ level, which might account for the absence of pulmonary edema in the humanized mice, although high viral loads and infiltrating lymphocytes were present in the brain and the lung. Recent findings suggested that patients with EV-A71 encephalitis have significantly higher frequencies of IL-8–251TT genotype and IL-8–251T alleles than patients with EV-A71-related HFMD without encephalitis, and patients with ANS dysregulation have higher plasma levels of IL-8 than patients with

pulmonary edema (32, 54). To the best of our knowledge, this is the first report showing that a level of human IL-8 was detected in the EV-A71-infected humanized mouse model. Importantly, human IL-8 is involved in leukocyte migration, in particular the recruitment of neutrophils. However, no true homologue for human IL-8 has been found in mice (55). Further elucidation of the precise role and mechanism of IL-8 may provide better insight into unraveling the modulation of immune responses during EV-A71 infection.

Collectively, we demonstrated that 4-week-old humanized mice were susceptible to infection with a non-mouse-adapted strain of EV-A71. From our results, EV-A71-infected humanized mice displayed limb weakness and paralysis, which were accompanied by a decrease in their neurobehavioral scores. The occurrence of pathogenic conditions in brain and spinal cord might be correlated to high viral loads in these organs. Notably, there was an increase in the number of activated human $CD4^+$ and $CD8^+$ T cells in the circulation and in the spleen, and the number of infiltrating T cells was elevated in the brain and the lung. The secretion of various proinflammatory cytokines, including human IFN-γ, IL-8, and IL-17A, was enhanced, which might contribute to the exacerbation of disease pathogenesis. Although pulmonary edema was not developed in our humanized mice, possibly due to inadequate proinflammatory cytokine levels, this mouse model allows us to delineate the modulation of immune responses during EV-A71 infection, which may provide a platform for the evaluation of anti-EV-A71 drug candidates in the future.

MATERIALS AND METHODS

Isolation of human $CD34^+$ cells. Human fetal livers were obtained from aborted fetuses at 15 to 23 weeks of gestation in strict accordance with the institutional ethical guidelines of KK Women's and Children's Hospital, Singapore, with written consent from the donors. SingHealth and National Health Care Group Research Ethics Committees Singapore specifically approved this study (IRB no. 2012/064/F). Fetal livers were processed and purified under sterile conditions with the use of a human CD34 positive selection kit (Stem Cell Technologies) as previously described (56).

Mice and transplantation of $CD34^+$ cells. NOD-*scid IL2Rγ*$^{-/-}$ (NSG) mice were purchased from The Jackson Laboratory and bred under specific-pathogen-free conditions at the Biological Resource Centre (BRC) at the Agency for Science, Technology and Research (A*STAR), Singapore. To generate humanized mice, 1- to 3-day-old NSG pups were sublethally irradiated at 1 Gy, and $CD34^+$ human fetal liver cells (2×10^5) were inoculated into the pups by intrahepatic injection. The presence of human $CD34^+$ stem cells was detected in bone marrow of the mice by fluorescence-activated cell sorting (FACS) analysis (data not shown), which was also shown in our previous study (57). All animal experiments were conducted in strict accordance to the *Guidelines of the Care and Use of Animals for Scientific Purposes*, which was released by the National Advisory Committee on Laboratory Animal Research, Agri-Food & Veterinary Authority of Singapore (58), and the International Animal Care and Use Committee (IACUC) at A*STAR. The IACUC specifically approved this study (IACUC no. 151060).

Cells and virus. Human rhabdomyosarcoma (RD) cells (ATCC CCL-136) were maintained in Dulbecco's modified minimal essential medium–Ham's F-12 (DMEM–F-12; Invitrogen), supplemented with 10% fetal bovine serum (FBS; Gibco), in a humidified incubator containing 5% CO_2 at 37°C. The EV-A71 strain (5865/SIN/00009; GenBank accession number AF316321; designated strain 41) belongs to the subgenogroup B4 and was isolated from a fatal case during the HFMD outbreak in Singapore in 2000 (59). EV-A71 was prepared by infecting monolayers of human RD cells and cultured in DMEM–F-12, supplemented with 2% FBS, in a humidified incubator containing 5% CO_2 at 37°C for 48 h. After incubation, human RD cells and supernatant were harvested, followed by three freeze-thaw cycles. Afterwards, the cell debris was removed by centrifugation at 10,000 × *g* at room temperature for 20 min.

Virus quantification. Human RD cell monolayer seeded in the well of a 24-well plate (Nunc) was infected with 10-fold serially diluted viral suspensions in DMEM–F-12 in a humidified incubator containing 5% CO_2 at 37°C for 1 h. After incubation, the cells were washed with phosphate-buffered saline (PBS) (pH 7.4) to remove unbound viral particles and overlaid with medium containing 2% FBS and 0.5% agarose. The cells were further incubated at 37°C for 48 h before they were fixed with 4% paraformaldehyde and stained with crystal violet. Plaques were counted visually and the infectious viral titer was calculated, expressed as the average number of PFU per milliliter of sample.

Mouse infection. Humanized mice and NSG mice of different ages were infected with EV-A71 by i.p. injection (10^8 PFU in 1 ml PBS/mouse). Total limb paralysis was used as a criterion for early euthanasia, and the mice were categorized as predicted to die (moribund mice) or predicted to survive (surviving mice) using the criteria described above.

Neurological evaluation. Neurobehavioral scores were blindly evaluated using a modified Garcia test as described elsewhere (60). The evaluation consists of seven tests, including beam balance (0 to 4), body proprioception (1 to 3), climbing (1 to 3), forepaw outstretching (0 to 3), spontaneous activity (0 to 3), symmetrical movement of all four limbs (0 to 3), and responsiveness to whisker stimulation (1 to 3).

The data are expressed as the average scores from three consecutive trials. Higher scores indicate better condition of the mice.

Hematoxylin and eosin staining and immunohistochemical staining. Mock-infected humanized mice and EV-A71-infected humanized mice were sacrificed at different time points. Brain, spinal cord, lung, and limb were harvested and fixed with 10% formalin (Sigma) at room temperature for 72 h. For H&E staining, the fixed tissues were paraffin embedded, sectioned (Leica), and stained with hematoxylin and eosin. The IHC staining was performed according to the manufacturers' instructions with the rabbit-specific IHC polymer detection kit HRP/DAB (Abcam) and mouse-on-mouse polymer IHC kit (Abcam). Stained images were captured using a ZEN fluorescence microscope (Zeiss) with ZEN 2 acquisition software (Zen Blue Version) and evaluated by a qualified pathologist in the Advanced Molecular Pathology Laboratory of IMCB.

Quantification of EV-A71 RNA in blood and various organs. Various organs from mock-infected humanized mice and EV-A71-infected humanized mice were harvested at different time points and homogenized in RPMI-1640 medium (Gibco) as described elsewhere (28). Viral RNA from serum and clarified homogenates from various organs were extracted using a QiaAmp viral RNA kit (Qiagen, Valencia, CA), and cDNA was synthesized using a QuantiTect reverse transcription kit (Qiagen) according to the manufacturer's instructions. The sequence of the forward primer is 5′-CCTCCGGCCCCTGAATGCG GCTAAT-3′, and the reverse primer is 5′-ATTGTCACCATAAGCAGCCA-3′. They were designed to amplify a 154-bp region in the VP1 gene in EV-A71. Quantitative reverse transcription-PCR (RT-PCR) was performed on a Bio-Rad iCycler IQ5 thermal cycler (Bio-Rad) using a QuantiTect SYBR green RT-PCR kit (Qiagen). A standard curve was constructed to quantify the viral RNA in the samples, which was generated using serially diluted EV-A71 viral stock.

Flow cytometry. Mononuclear cells (MNC) were stained with LIVE/DEAD fixable blue stain (Sigma) at room temperature for 30 min prior to staining with the following antibodies at 4°C for 20 min: anti-mouse CD45.1 antibody (Becton, Dickinson), anti-human CD3 (Becton, Dickinson), anti-human CD4 (Becton, Dickinson), anti-human CD8 (Becton, Dickinson), anti-human CD14 (BioLegend), anti-human CD19 (Becton, Dickinson), anti-human CD34 (Miltenyi Biotec), anti-human CD45 (BioLegend), anti-human CD56 (BioLegend), anti-human CD69 (BioLegend), anti-human CD133 (Miltenyi Biotec), and anti-human HLA-DR (Becton, Dickinson). Flow cytometric analysis was performed on an LSRII flow cytometer using FACSDiva software (Becton, Dickinson). A total of 10,000 events were collected per sample and analyzed using FlowJo software 7.5.5 (TreeStar).

Human IFN-γ T cell ELISPOT assay. ELISPOT assay was performed according to the manufacturer's instructions (U-CyTech BioSciences). In brief, splenocytes were isolated from mock-infected humanized mice and EV-A71-infected humanized mice at 9 weeks postinfection and were resuspended in RPMI 1640 medium. Splenocytes (4×10^6 cells/well) seeded in the well of a 24-well plate were preincubated with UV-inactivated EV-A71 in a humidified incubator containing 5% CO_2 at 37°C for 24 h. After incubation, splenocytes were washed three times with serum-free RPMI 1640 medium, and the splenocytes (10^4 cells/well) were further incubated with UV-inactivated EV-A71 (10^6 PFU/well) in a precoated 96-well ELISPOT plate in a humidified incubator containing 5% CO_2 at 37°C for 72 h. Splenocytes stimulated with PHA were used as a positive control. The number of spots in each well, which represents the human IFN-γ-producing cells, was counted using an ELISPOT reader (Bioreader 4000 Pro-B; Biosys). The data are expressed as spot-forming units per 10^4 splenocytes.

Isolation of mononuclear cells from various organs in humanized mice. Brain and lung of mock-infected humanized mice and EV-A71-infected humanized mice were harvested at 9 weeks postinfection, and MNC were isolated as previously described, with slight modifications (56). In brief, brain tissue was cut into small pieces and meshed in RPMI 1640 medium. Lung tissue was cut into small pieces and digested with collagenase IV (0.8 mg/ml; Worthington), supplemented with DNase I (1 μg/ml; Roche), in a humidified incubator containing 5% CO_2 at 37°C for 1 h. Afterwards, cells from the brain and lung were filtered through a 70-μm cell strainer (Fisher Scientific) and centrifuged at $300 \times g$ for 5 min. The cell pellet was resuspended in RPMI 1640 medium, overlaid on 35% Percoll-PBS solution (GE Healthcare), and centrifuged at $1,200 \times g$ for 20 min without braking. MNC were collected as the cell pellet, which was resuspended in RPMI 1640 for subsequent flow cytometric analysis.

Cytokine quantification. Cytokine levels in the serum from mock-infected humanized mice and EV-A71-infected humanized mice was determined by a LEGENDplex human inflammation panel (13-plex) (BioLegend) according to the manufacturer's instructions. The cytokine profile was analyzed by flow cytometry (LSRII; Becton, Dickinson) and LEGENDplex data analysis software (BioLegend).

Statistical analysis. All statistical analyses were performed using GraphPad Prism (GraphPad, Inc.), and the data are expressed as means $\pm$ standard errors of the means (SEM). Kaplan-Meier survival curves were analyzed by a log-rank test, while unpaired Student's *t* test was used for statistical analysis between mock-infected humanized mice and EV-A71-infected humanized mice for other experiments. The differences are considered statistically significant at a *P* value of <0.05.

ACKNOWLEDGMENTS

This study was supported by the National Research Foundation Fellowship Singapore (NRF-NRFF2017-03) to Q.C. and by the Eradication of HBV TCR Program (NMRC/TCR/014-NUHS/2015), National Medical Research Council, Singapore. The study was also supported by the Key Laboratory of Functional and Clinical Translational Medicine, Fujian Province University (JNYLC1811). The funders had no role in study design, data collection and interpretation, or the decision to submit the work for publication.

We thank the Advanced Molecular Pathology Laboratory of IMCB for offering pathological consultations and support.

Y.K. and W.N.L. designed and performed experiments, analyzed and interpreted data, and prepared the manuscript; Z.H., M.L., S.Y.T., Y.W.T., and X.Y.C. performed experiments; Y.F., E.K.H., H.C., K.T.E.C., and J.K.Y.C. contributed to experimental design and prepared the manuscript; J.J.H.C. designed the experiments and supervised the project; Q.C. conceived the study, designed the experiments, supervised the project, and prepared the manuscript.

We have no competing financial interests to declare.

REFERENCES

1. Pathinayake PS, Hsu AC, Wark PA. 2015. Innate immunity and immune evasion by enterovirus 71. Viruses 7:6613–6630. https://doi.org/10.3390/v7122961.
2. McMinn PC. 2002. An overview of the evolution of enterovirus 71 and its clinical and public health significance. FEMS Microbiol Rev 26:91–107. https://doi.org/10.1111/j.1574-6976.2002.tb00601.x.
3. Schmidt NJ, Lennette EH, Ho HH. 1974. An apparently new enterovirus isolated from patients with disease of the central nervous system. J Infect Dis 129:304–309. https://doi.org/10.1093/infdis/129.3.304.
4. Ding NZ, Wang XM, Sun SW, Song Q, Li SN, He CQ. 2009. Appearance of mosaic enterovirus 71 in the 2008 outbreak of China. Virus Res 145:157–161. https://doi.org/10.1016/j.virusres.2009.06.006.
5. Fan X, Jiang J, Liu Y, Huang X, Wang P, Liu L, Wang J, Chen W, Wu W, Xu B. 2013. Detection of human enterovirus 71 and coxsackievirus A16 in an outbreak of hand, foot, and mouth disease in Henan Province, China in 2009. Virus Genes 46:1–9. https://doi.org/10.1007/s11262-012-0814-x.
6. Chen JF, Zhang RS, Ou XH, Chen FM, Sun BC. 2014. The role of enterovirus 71 and coxsackievirus A strains in a large outbreak of hand, foot, and mouth disease in 2012 in Changsha, China. Int J Infect Dis 28:17–25. https://doi.org/10.1016/j.ijid.2014.07.024.
7. Cho HK, Lee NY, Lee H, Kim HS, Seo JW, Hong YM, Lee SJ, Lee SW, Cheon DS, Hong JY, Kang BH, Kim JH, Kim KH. 2010. Enterovirus 71-associated hand, foot and mouth diseases with neurologic symptoms, a university hospital experience in Korea, 2009. Korean J Pediatr 53:639–643. https://doi.org/10.3345/kjp.2010.53.5.639.
8. Ma E, Chan KC, Cheng P, Wong C, Chuang SK. 2010. The enterovirus 71 epidemic in 2008–public health implications for Hong Kong. Int J Infect Dis 14:e775. https://doi.org/10.1016/j.ijid.2010.02.2265.
9. Hsu BM, Chen CH, Wan MT. 2007. Genetic diversity of epidemic enterovirus 71 strains recovered from clinical and environmental samples in Taiwan. Virus Res 126:69–75. https://doi.org/10.1016/j.virusres.2007.01.018.
10. Ho M, Chen ER, Hsu KH, Twu SJ, Chen KT, Tsai SF, Wang JR, Shih SR. 1999. An epidemic of enterovirus 71 infection in Taiwan. Taiwan Enterovirus Epidemic Working Group. N Engl J Med 341:929–935. https://doi.org/10.1056/NEJM199909233411301.
11. Huang CC, Liu CC, Chang YC, Chen CY, Wang ST, Yeh TF. 1999. Neurologic complications in children with enterovirus 71 infection. N Engl J Med 341:936–942. https://doi.org/10.1056/NEJM199909233411302.
12. Wang SM, Liu CC. 2014. Update of enterovirus 71 infection: epidemiology, pathogenesis and vaccine. Expert Rev Anti Infect Ther 12:447–456. https://doi.org/10.1586/14787210.2014.895666.
13. McMinn P, Stratov I, Nagarajan L, Davis S. 2001. Neurological manifestations of enterovirus 71 infection in children during an outbreak of hand, foot, and mouth disease in Western Australia. Clin Infect Dis 32:236–242. https://doi.org/10.1086/318454.
14. Chumakov M, Voroshilova M, Shindarov L, Lavrova I, Gracheva L, Koroleva G, Vasilenko S, Brodvarova I, Nikolova M, Gyurova S, Gacheva M, Mitov G, Ninov N, Tsylka E, Robinson I, Frolova M, Bashkirtsev V, Martiyanova L, Rodin V. 1979. Enterovirus 71 isolated from cases of epidemic poliomyelitis-like disease in Bulgaria. Arch Virol 60:329–340. https://doi.org/10.1007/BF01317504.
15. Huang WC, Shih WL, Yang SC, Yen TY, Lee JT, Huang YC, Li CC, Hsieh YC, Lin TY, Chang LY, Huang LM. 2017. Predicting severe enterovirus 71 infection: age, comorbidity, and parental behavior matter. J Microbiol Immunol Infect 50:10–16. https://doi.org/10.1016/j.jmii.2014.11.013.
16. Omana-Cepeda C, Martinez-Valverde A, del Mar Sabater-Recolons M, Jane-Salas E, Mari-Roig A, Lopez-Lopez J. 2016. A literature review and case report of hand, foot and mouth disease in an immunocompetent adult. BMC Res Notes 9:165. https://doi.org/10.1186/s13104-016-1973-y.
17. Wang YF, Yu CK. 2014. Animal models of enterovirus 71 infection: applications and limitations. J Biomed Sci 21:31. https://doi.org/10.1186/1423-0127-21-31.
18. Zhang Y, Cui W, Liu L, Wang J, Zhao H, Liao Y, Na R, Dong C, Wang L, Xie Z, Gao J, Cui P, Zhang X, Li Q. 2011. Pathogenesis study of enterovirus 71 infection in rhesus monkeys. Lab Investig 91:1337–1350. https://doi.org/10.1038/labinvest.2011.82.
19. Zhongping X, Hua L, Ting Y, Zhengling L, Min F, Tianhong X, Runxiang L, Dong S, Guangju J, Lei Y, Rong Y, Fangyu L, Qihan L. 2016. Biological characteristics of different epidemic enterovirus 71 strains and their pathogeneses in neonatal mice and rhesus monkeys. Virus Res 213:82–89. https://doi.org/10.1016/j.virusres.2015.11.007.
20. Wang W, Duo J, Liu J, Ma C, Zhang L, Wei Q, Qin C. 2011. A mouse muscle-adapted enterovirus 71 strain with increased virulence in mice. Microbes Infect 13:862–870. https://doi.org/10.1016/j.micinf.2011.04.004.
21. Chen IC, Wang SM, Yu CK, Liu CC. 2013. Subneutralizing antibodies to enterovirus 71 induce antibody-dependent enhancement of infection in newborn mice. Med Microbiol Immunol 202:259–265. https://doi.org/10.1007/s00430-013-0289-y.
22. Chang J, Li J, Liu X, Liu G, Yang J, Wei W, Zhang W, Yu XF. 2015. Broad protection with an inactivated vaccine against primary-isolated lethal enterovirus 71 infection in newborn mice. BMC Microbiol 15:139. https://doi.org/10.1186/s12866-015-0474-9.
23. Chen HL, Wang LC, Chang CH, Yen CC, Cheng WT, Wu SC, Hung CM, Kuo MF, Chen CM. 2008. Recombinant porcine lactoferrin expressed in the milk of transgenic mice protects neonatal mice from a lethal challenge with enterovirus type 71. Vaccine 26:891–898. https://doi.org/10.1016/j.vaccine.2007.12.013.
24. Huang SW, Lee YP, Hung YT, Lin CH, Chuang JI, Lei HY, Su IJ, Yu CK. 2011. Exogenous interleukin-6, interleukin-13, and interferon-gamma provoke pulmonary abnormality with mild edema in enterovirus 71-infected mice. Respir Res 12:147. https://doi.org/10.1186/1465-9921-12-147.
25. Lin TY, Chang LY, Huang YC, Hsu KH, Chiu CH, Yang KD. 2002. Different proinflammatory reactions in fatal and non-fatal enterovirus 71 infections: implications for early recognition and therapy. Acta Paediatr 91:632–635. https://doi.org/10.1111/j.1651-2227.2002.tb03292.x.
26. Lin TY, Hsia SH, Huang YC, Wu CT, Chang LY. 2003. Proinflammatory cytokine reactions in enterovirus 71 infections of the central nervous system. Clin Infect Dis 36:269–274. https://doi.org/10.1086/345905.
27. Wang SM, Lei HY, Huang KJ, Wu JM, Wang JR, Yu CK, Su IJ, Liu CC. 2003. Pathogenesis of enterovirus 71 brainstem encephalitis in pediatric patients: roles of cytokines and cellular immune activation in patients with pulmonary edema. J Infect Dis 188:564–570. https://doi.org/10.1086/376998.
28. Khong WX, Yan B, Yeo H, Tan EL, Lee JJ, Ng JK, Chow VT, Alonso S. 2012. A non-mouse-adapted enterovirus 71 (EV71) strain exhibits neurotropism, causing neurological manifestations in a novel mouse model of EV71 infection. J Virol 86:2121–2131. https://doi.org/10.1128/JVI.06103-11.
29. Solomon T, Lewthwaite P, Perera D, Cardosa MJ, McMinn P, Ooi MH. 2010. Virology, epidemiology, pathogenesis, and control of enterovirus 71. Lancet Infect Dis 10:778–790. https://doi.org/10.1016/S1473-3099(10)70194-8.
30. Chen CY, Chang YC, Huang CC, Lui CC, Lee KW, Huang SC. 2001. Acute flaccid paralysis in infants and young children with enterovirus 71

infection: MR imaging findings and clinical correlates. Am J Neuroradiol 22:200–205.
31. Lin YW, Chang KC, Kao CM, Chang SP, Tung YY, Chen SH. 2009. Lymphocyte and antibody responses reduce enterovirus 71 lethality in mice by decreasing tissue viral loads. J Virol 83:6477–6483. https://doi.org/10.1128/JVI.00434-09.
32. Wang SM, Lei HY, Liu CC. 2012. Cytokine immunopathogenesis of enterovirus 71 brain stem encephalitis. Clin Dev Immunol 2012:876241. https://doi.org/10.1155/2012/876241.
33. Chen J, Tong J, Liu H, Liu Y, Su Z, Wang S, Shi Y, Zheng D, Sandoghchian S, Geng J, Xu H. 2012. Increased frequency of Th17 cells in the peripheral blood of children infected with enterovirus 71. J Med Virol 84:763–767. https://doi.org/10.1002/jmv.23254.
34. Ryu WS, Kang B, Hong J, Hwang S, Kim J, Cheon DS. 2010. Clinical and etiological characteristics of enterovirus 71-related diseases during a recent 2-year period in Korea. J Clin Microbiol 48:2490–2494. https://doi.org/10.1128/JCM.02369-09.
35. Yi EJ, Shin YJ, Kim JH, Kim TG, Chang SY. 2017. Enterovirus 71 infection and vaccines. Clin Exp Vaccine Res 6:4–14. https://doi.org/10.7774/cevr.2017.6.1.4.
36. Fang CY, Liu CC. 2018. Recent development of enterovirus A vaccine candidates for the prevention of hand, foot, and mouth disease. Expert Rev Vaccines 17:819–831. https://doi.org/10.1080/14760584.2018.1510326.
37. Li G, Gao Q, Yuan S, Wang L, Altmeyer R, Lan K, Yin F, Zou G. 2017. Characterization of three small molecule inhibitors of enterovirus 71 identified from screening of a library of natural products. Antiviral Res 143:85–96. https://doi.org/10.1016/j.antiviral.2017.04.006.
38. Caine EA, Partidos CD, Santangelo JD, Osorio JE. 2013. Adaptation of enterovirus 71 to adult interferon deficient mice. PLoS One 8:e59501. https://doi.org/10.1371/journal.pone.0059501.
39. Caine EA, Moncla LH, Ronderos MD, Friedrich TC, Osorio JE. 2016. A single mutation in the VP1 of enterovirus 71 is responsible for increased virulence and neurotropism in adult interferon-deficient mice. J Virol 90:8592–8604. https://doi.org/10.1128/JVI.01370-16.
40. Weng KF, Chen LL, Huang PN, Shih SR. 2010. Neural pathogenesis of enterovirus 71 infection. Microbes Infect 12:505–510. https://doi.org/10.1016/j.micinf.2010.03.006.
41. Cheng HY, Huang YC, Yen TY, Hsia SH, Hsieh YC, Li CC, Chang LY, Huang LM. 2014. The correlation between the presence of viremia and clinical severity in patients with enterovirus 71 infection: a multi-center cohort study. BMC Infect Dis 14:417. https://doi.org/10.1186/1471-2334-14-417.
42. Ren R, Racaniello VR. 1992. Poliovirus spreads from muscle to the central nervous system by neural pathways. J Infect Dis 166:747–752. https://doi.org/10.1093/infdis/166.4.747.
43. Chang LY, Hsiung CA, Lu CY, Lin TY, Huang FY, Lai YH, Chiang YP, Chiang BL, Lee CY, Huang LM. 2006. Status of cellular rather than humoral immunity is correlated with clinical outcome of enterovirus 71. Pediatr Res 60:466–471. https://doi.org/10.1203/01.pdr.0000238247.86041.19.
44. Wu J, Cui D, Yang X, Lou J, Lin J, Ye X, Qin Z, Huang L, Zhao D, Huo Z, Xie G, Zheng S, Yu F, Lu L, Chen Y. 2014. Increased frequency of circulating follicular helper T cells in children with hand, foot, and mouth disease caused by enterovirus 71 infection. J Immunol Res 2014:651872. https://doi.org/10.1155/2014/651872.
45. Li S, Cai C, Feng J, Li X, Wang Y, Yang J, Chen Z. 2014. Peripheral T lymphocyte subset imbalances in children with enterovirus 71-induced hand, foot and mouth disease. Virus Res 180:84–91. https://doi.org/10.1016/j.virusres.2013.11.021.
46. Cui D, Zhong F, Lin J, Wu Y, Long Q, Yang X, Zhu Q, Huang L, Mao Q, Huo Z, Zhou Z, Xie G, Zheng S, Yu F, Chen Y. 2017. Changes of circulating Th22 cells in children with hand, foot, and mouth disease caused by enterovirus 71 infection. Oncotarget 8:29370–29382. https://doi.org/10.18632/oncotarget.14083.
47. Viallard JF, Bloch-Michel C, Neau-Cransac M, Taupin JL, Garrigue S, Miossec V, Mercie P, Pellegrin JL, Moreau JF. 2001. HLA-DR expression on lymphocyte subsets as a marker of disease activity in patients with systemic lupus erythematosus. Clin Exp Immunol 125:485–491. https://doi.org/10.1046/j.1365-2249.2001.01623.x.
48. Nakayama M, Takeda K, Kawano M, Takai T, Ishii N, Ogasawara K. 2011. Natural killer (NK)-dendritic cell interactions generate MHC class II-dressed NK cells that regulate CD4+ T cells. Proc Natl Acad Sci U S A 108:18360–18365. https://doi.org/10.1073/pnas.1110584108.
49. Wang J, Pu J, Huang H, Zhang Y, Liu L, Yang E, Zhou X, Ma N, Zhao H, Wang L, Xie Z, Tang D, Li Q. 2013. EV71-infected CD14(+) cells modulate the immune activity of T lymphocytes in rhesus monkeys. Emerg Microbes Infect 2:e44. https://doi.org/10.1038/emi.2013.44.
50. Hsiao HB, Chou AH, Lin SI, Lien SP, Liu CC, Chong P, Chen CY, Tao MH, Liu SJ. 2014. Delivery of human EV71 receptors by adeno-associated virus increases EV71 infection-induced local inflammation in adult mice. Biomed Res Int 2014:878139. https://doi.org/10.1155/2014/878139.
51. Wang SM, Lei HY, Su LY, Wu JM, Yu CK, Wang JR, Liu CC. 2007. Cerebrospinal fluid cytokines in enterovirus 71 brain stem encephalitis and echovirus meningitis infections of varying severity. Clin Microbiol Infect 13:677–682. https://doi.org/10.1111/j.1469-0691.2007.01729.x.
52. Corbin JG, Kelly D, Rath EM, Baerwald KD, Suzuki K, Popko B. 1996. Targeted CNS expression of interferon-gamma in transgenic mice leads to hypomyelination, reactive gliosis, and abnormal cerebellar development. Mol Cell Neurosci 7:354–370. https://doi.org/10.1006/mcne.1996.0026.
53. Wang LC, Chen SO, Chang SP, Lee YP, Yu CK, Chen CL, Tseng PC, Hsieh CY, Chen SH, Lin CF. 2015. Enterovirus 71 proteins 2A and 3D antagonize the antiviral activity of gamma interferon via signaling attenuation. J Virol 89:7028–7037. https://doi.org/10.1128/JVI.00205-15.
54. Li J, Lin A, Yu C, Zhang Z, Xu D, Hu W, Liu L, Wang S, Nie X, Sun W, Gai Z, Chen Z. 2015. Association of enterovirus 71 encephalitis with the interleukin-8 gene region in Chinese children. Infect Dis (Lond) 47:418–422. https://doi.org/10.3109/00365548.2015.1007473.
55. Becker MD, O'Rourke LM, Blackman WS, Planck SR, Rosenbaum JT. 2000. Reduced leukocyte migration, but normal rolling and arrest, in interleukin-8 receptor homologue knockout mice. Investig Ophthalmol Vis Sci 41:1812–1817.
56. Chen Q, Ye W, Jian Tan W, Mei Yong KS, Liu M, Qi Tan S, Loh E, Te Chang K, Chye Tan T, Preiser PR, Chen J. 2015. Delineation of natural killer cell differentiation from myeloid progenitors in human. Sci Rep 5:15118. https://doi.org/10.1038/srep15118.
57. Yong KS, Keng CT, Tan SQ, Loh E, Chang KT, Tan TC, Hong W, Chen Q. 2016. Human CD34(lo)CD133(lo) fetal liver cells support the expansion of human CD34(hi)CD133(hi) hematopoietic stem cells. Cell Mol Immunol 13:605–614. https://doi.org/10.1038/cmi.2015.40.
58. National Advisory Committee on Laboratory Animal Research. 2004. Guidelines of the care and use of animals for scientific purpose. National Advisory Committee on Laboratory Animal Research, Agri-Food & Veterinary Authority of Singapore, Singapore.
59. Singh S, Poh CL, Chow VT. 2002. Complete sequence analyses of enterovirus 71 strains from fatal and non-fatal cases of the hand, foot and mouth disease outbreak in Singapore (2000). Microbiol Immunol 46:801–808. https://doi.org/10.1111/j.1348-0421.2002.tb02767.x.
60. Chen S, Zhu Z, Klebe D, Bian H, Krafft PR, Tang J, Zhang J, Zhang JH. 2014. Role of P2X purinoceptor 7 in neurogenic pulmonary edema after subarachnoid hemorrhage in rats. PLoS One 9:e89042. https://doi.org/10.1371/journal.pone.0089042.